Optical beam classification using deep learning: A comparison with rule- and feature-based classification

Md. Zahangir Alom[ab], Abdul A. S. Awwal[b], Roger Lowe-Webb, Tarek M. Taha[a]
[a]Department of Electrical and Computer Engineering, University of Dayton, Dayton, Ohio 45469;
[b]National Ignition Facility (NIF), Lawrence Livermore National Laboratory, Livermore, California 94551.

ABSTRACT

Deep-learning methods are gaining popularity because of their state-of-the-art performance in image classification tasks. In this paper, we explore classification of laser-beam images from the National Ignition Facility (NIF) using a novel deep-learning approach. NIF is the world's largest, most energetic laser. It has nearly 40,000 optics that precisely guide, reflect, amplify, and focus 192 laser beams onto a fusion target. NIF utilizes four petawatt lasers called the Advanced Radiographic Capability (ARC) to produce backlighting X-ray illumination to capture implosion dynamics of NIF experiments with picosecond temporal resolution. In the current operational configuration, four independent short-pulse ARC beams are created and combined in a split-beam configuration in each of two NIF apertures at the entry of the pre-amplifier. The sub-aperture beams then propagate through the NIF beampath up to the ARC compressor. Each ARC beamlet is separately compressed with a dedicated set of four gratings and recombined as sub-apertures for transport to the parabola vessel, where the beams are focused using parabolic mirrors and pointed to the target. Small angular errors in the compressor gratings can cause the sub-aperture beams to diverge from one another and prevent accurate alignment through the transport section between the compressor and parabolic mirrors. This is an off-normal condition that must be detected and corrected. The goal of the off-normal check is to determine whether the ARC beamlets are sufficiently overlapped into a merged single spot or diverged into two distinct spots. Thus, the objective of the current work is three-fold: developing a simple algorithm to perform off-normal classification, exploring the use of Convolutional Neural Network (CNN) for the same task, and understanding the inter-relationship of the two approaches. The CNN recognition results are compared with other machine-learning approaches, such as Deep Neural Network (DNN) and Support Vector Machine (SVM). The experimental results show around 96% classification accuracy using CNN; the CNN approach also provides comparable recognition results compared to the present feature-based off-normal detection. The feature-based solution was developed to capture the expertise of a human expert in classifying the images. The misclassified results are further studied to explain the differences and discover any discrepancies or inconsistencies in current classification.

Keywords: Deep Learning, CNN, DBN, SVM, feature extraction, beam classification.

1. INTRODUCTION

The National Ignition Facility (NIF) is the world's largest, most energetic laser. It has nearly 40,000 optics that precisely guide, reflect, amplify, and focus 192 laser beams onto a fusion target, and thus provides a platform for performing high-energy laser physics experiments [1,2]. A diagnostic known as the Advanced Radiographic Capability (ARC) was developed to properly understand the implosion dynamics [3,4]. ARC produces backlighting high-energy X-ray beams that can penetrate and image the implosion as it is happening. Currently, four independent short-pulse ARC beams are created and combined in a split-beam configuration in each of two NIF apertures at the entry of the pre-amplifier. The sub-aperture beams are amplified using NIF hardware as they propagate through the NIF beampath up to the ARC compressor. Each ARC beamlet is separately compressed with a set of four gratings and recombined as sub-apertures for transport to the parabola vessel, where the beams are focused using parabolic mirrors and pointed to the target. Small angular deviations in the compressor gratings can introduce pointing errors in the sub-aperture beams and cause them to diverge from one another. This prevents accurate alignment through the transport section between the compressor and parabolic mirrors. This off-normal condition must be identified using Automatic Alignment (AA) algorithms [5] and corrected before continuing with the ARC shot [6]. The off-normal check determines whether the ARC beamlets are merged into a single spot or have diverged into two distinct spots. Typical examples of single- and double-spot ARC alignment beam images and the ARC beamlets are shown in Figure 1.

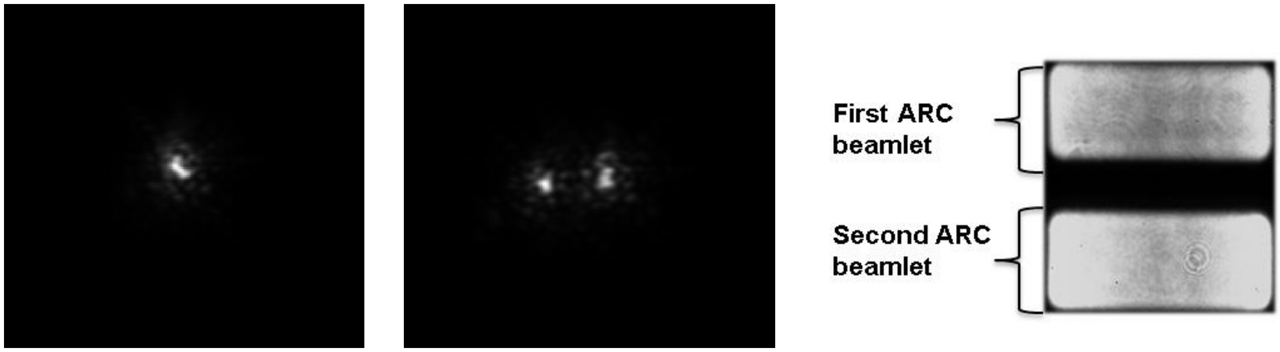

(a) (b) (c)

Figure 1. Example of ARC (a) single-spot and (b) double-spot far-field alignment beam images; (c) Near-field image of the ARC beamlets

For this paper, a feature-based learning system was developed to identify the two spots' off-normal condition. The feature-based solution was gradually learned with the help of a human subject matter expert. Additionally, we explore the above classification task using novel deep-learning approaches: Convolutional Neural Network (CNN) [7,8], Deep Neural Network (DNN) [9] and Support Vector Machine (SVM) [10]. The misclassified results are further studied to explain the differences and discover any discrepancies or inconsistencies in current classification.

The rest of the paper has been organized as follows: Section 2 discusses the present feature-based approach for off-normal classification of laser beams. The theoretical details of different deep-learning techniques are presented in Section 3. Section 4 shows the details of the experimental results and analysis, followed by conclusions in the final section.

2. FEATURE-BASED LEARNING SYSTEM

The set of NIF ARC images consists of 372 images. We visually examined the image set and determined that it contained three types of images. One class of images depicts a single spot; another class contains double spots, and the rest appear to be more than two spots or a collection of diffracted spots. In building the algorithm, the simple cases were classified first using binarization and feature analysis. If the binarization produced a single spot, it was classified as one spot. If binarization produced two spots, it was categorized as a double-spot image. However, the two- or single-spot classification depends on the intensity level at which binarization was performed. Therefore, it was important to set the initial intensity level for examining the image carefully. Since the second spot was originally expected to be equally bright, after some experimentation the binarization threshold was set to 64% of the peak intensity as shown in Fig. 2.

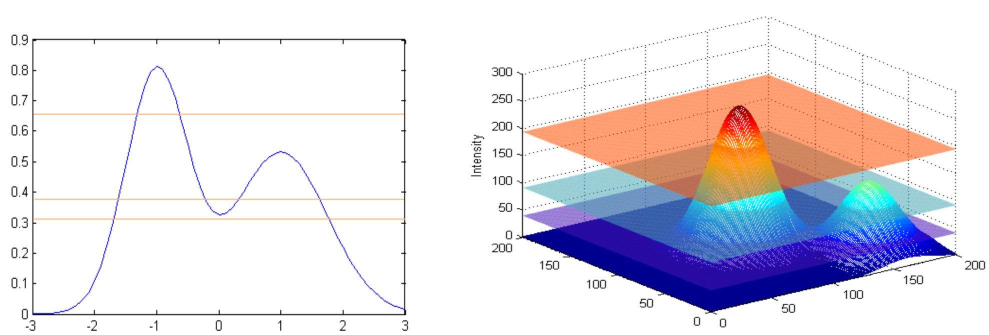

Figure 2. Thresholding approaches for different tests

To ensure that the second spot was not a spurious noise signal but a viable spot, three parameters were examined: the energy ratio, the blob-size ratio, and the separation between the spots. During the initial learning phase of the feature-based classification, we set the following restrictions on the allowable two-spot characteristics:

Number of spots = 2
Energy Ratio > 25% (ratio of energy of the second highest sized blob to the highest intensity blob)
Blob Ratio > 30% (ratio of sizes)
Separation > 13 pixels (distance between the centroids of the two blobs)

This first classification attempt, called Test 1 and shown in Figure 3, classified 30% of the images and missed many more. The condition was augmented by additional conditions, such as the number of spots equals 4 where the 4^{th} spot had fewer than 10 pixels. At the same time, a human expert was consulted.

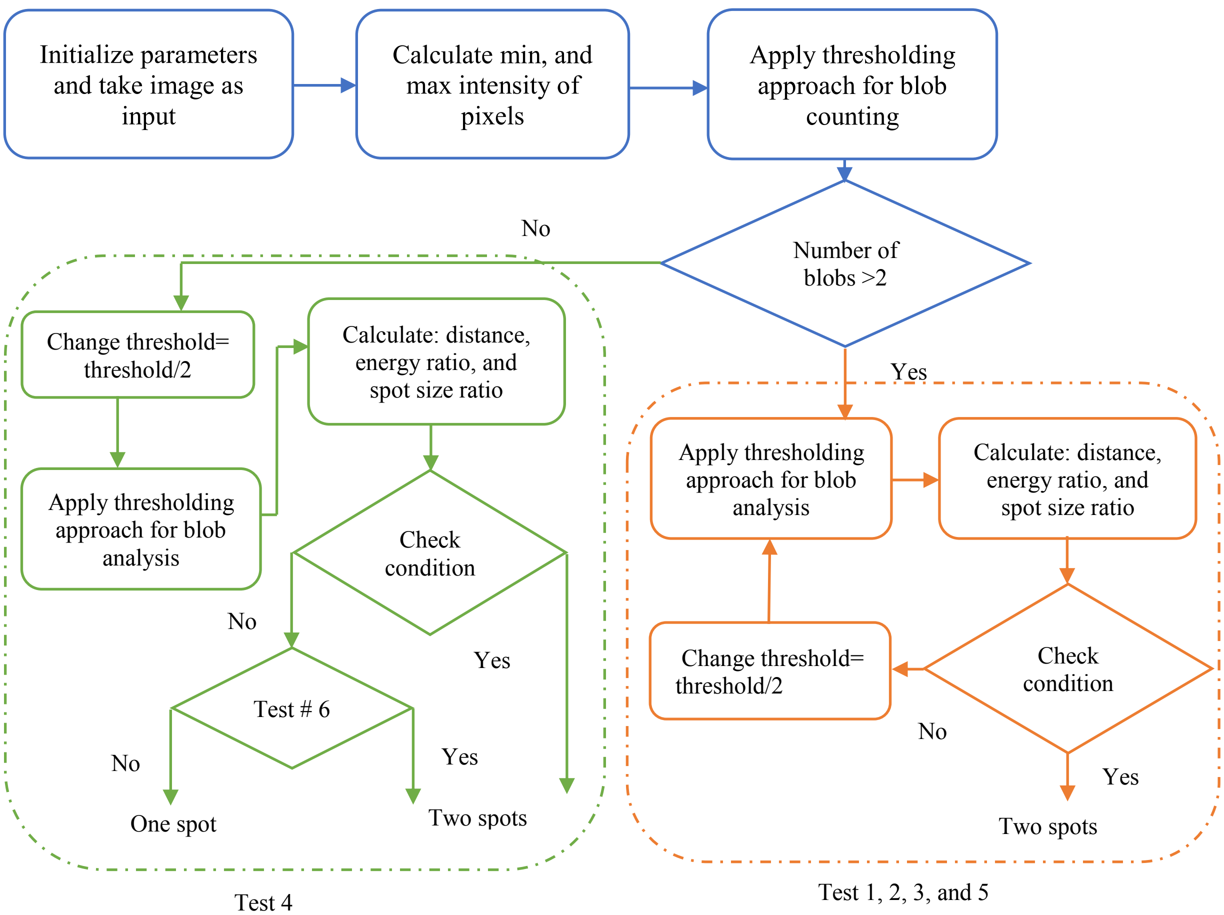

Figure 3. Flowchart of feature-extraction-based approach for beam classification

When the additional conditions failed to detect some of the two-spot images, the threshold was reduced to half of the original threshold. Tests were then performed using similar values of the three parameters: these were tests 2, 3 and 5. The goal was to detect as many obvious two-spot images as possible. Decreasing the binarization threshold from 64% to 32% of the peak intensity resulted in 15% of the images being detected using tests 1,2,3,4, and 5.

There were some cases, however, that could still not be detected with tests 1 to 5. After consulting a human expert and obtaining the recommended classes, additional conditions were added to bring the missed examples into the class. The additional test is based on the observation that, as shown in Figure 2, it is possible for both 64% and its half threshold to fail to detect two spots because at those thresholds only a single binary object is detected. An additional test (Test 6) was added which divided the interval of the two thresholds into ten steps and looked for two spots. Test 6 assigned 55% of the remaining images and sorted them into the proper classes. Thus tests 1-6 provided classification of 100% of the images.

3. DEEP-LEARNING METHODS

3.1 Convolutional Neural Network (CNN)

The CNN architecture was proposed by Fukushima in 1980 [11]. It was not widely used, however, because the training algorithm required high computational power. In 1998, Lacuna *et al*. applied a gradient-based learning algorithm to CNN and obtained successful results in different application domains including image processing, computer vision, machine learning, and others [7,8,12].

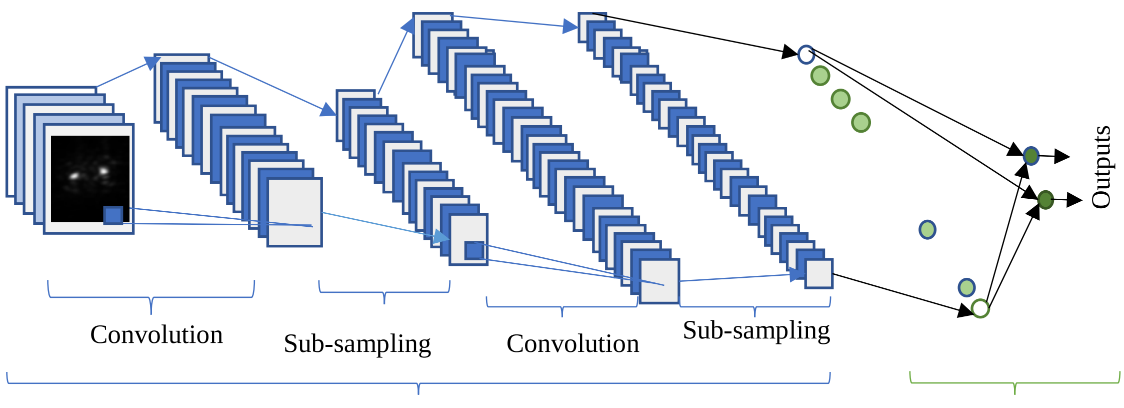

Figure 4. The overall architecture of the CNN used in this work, which includes an input layer, multiple alternating convolution and sub-sampling (pooling) layers, and one fully connected classification layer.

Figure 4 shows the overall architecture of the CNN, which consists of two main parts: feature extractor and classifier. In the feature extraction layers, each layer of the network receives the output from the immediate previous layer as its input and passes its output as an input to the next layer. The CNN architecture is composed of the combination of three types of layers: convolution, sub-sampling (pooling), and classification. Convolution and max-pooling are two types of layers in the low and middle levels of the network. The even-numbered layers are for convolution, and the odd-numbered layers work for max-pooling operation. Each node of the convolution layer extracts the features from the input images by convolution operation on the input nodes. The sub-sampling (pooling) layer abstracts the feature through average or propagating the operation on input nodes. The output nodes of the convolution and max-pooling layers are grouped into a 2D plane, which is called feature mapping. Each plane of the layer is usually derived with the combination of one or more planes of the previous layers. The node of the plane is connected to a small region of each connected plane of the previous layer.

The higher-level features have been derived from the propagated features of the lower-level layers. As the feature propagates to the highest layer or level, the dimension of the feature is reduced depending on the size of the convolutional and max-pooling masks, respectively. The number of mapped features usually is increased, however, for selecting or mapping the extreme suitable features of the input images for better classification accuracy. The outputs of the last layer of CNN are used as inputs to the fully connected neural network, which is called the classification layer. The feed-forward neural networks are used as a classifier in this work because they already have proven to perform better compared to others [9,13]. In the classification layer, all the features from the feature extraction layer are connected as inputs to the fully connected layer. Sometimes feature selection techniques have been applied [12] from selecting the desired number of nodes from the CNN's output layer. The score of the respective class has been calculated in the top classification layer using the softmax layer. Based on the highest score, the classifier gives outputs for the corresponding classes after finishing the propagation. Mathematical details on different layers of CNN are discussed in the following section.

3.1.1 Convolutional layer

In this layer, the feature maps of the previous layer are convolved with a learnable kernel such as random or Gabor. In this implementation, random filters are used. The outputs of the kernel go through linear or non-linear activation functions of Rectified Linear Unit (ReLU) to form the output feature maps. Each of the output feature maps can be combined with more than one input feature map. In general, we have that

$$x_j^l = f\left(\sum_{i \epsilon M_j} x_i^{l-1} * k_{ij}^l + b_j^l\right) \quad (1)$$

where x_j^l is the output of the current layer, x_i^{l-1} is previous layer output, k_{ij}^l is the kernel for the present layer, and b_j^l is the bias for the current layer. M_j represents a selection of input maps. For each output map is given an additive bias b. The input maps, however, will be convolved with distinct kernels to generate the corresponding output maps.

3.1.2 Subsampling layer

The subsampling layer performs down sampling operations on the input maps. In this layer, the input and output maps do change. Due to the down sampling operation, the size of the output maps will be reduced depending on the size of the down sampling mask. In this experiment, 2×2 down sampling masks have been used. If there are N input maps, then there will be exactly N output maps. This operation can be formulated as

$$\mathrm{x}_j^l = \mathrm{f}\left(\beta_j^l \, \mathrm{down}\left(\mathrm{x}_j^{l-1}\right) + \mathrm{b}_j^l\right) \quad (2)$$

where down $(.)$ represents a sub-sampling function. This function usually sums up over $n \times n$ blocks of the maps from the previous layers and selects the average value or selects the highest values among the $n \times n$ block maps. Therefore, the output map dimension has been reduced n times with respect to both dimensions. The output map will be added with bias b. Finally, the outputs go through a linear or non-linear activation function.

3.1.3 Classification layer

This is the fully connected layer which computes the score of each class from the extracted features from the convolutional layer in the preceding steps. In this work, the size of the feature maps for the fully connected layer one 5×5×12. The final layer feature maps have been considered as scalar values which passed to the fully connected layers, and a feed-forward neural approach has been used for the classification. As for the activation function, the softmax function is employed in this implementation.

In the backward propagation through of the CNNs, the filters have been updated for the convolution layer by performing the convolutional operation between the convolutional layer and the immediate previous layer on the feature maps. The change of the weight matrix for the neural network layer is calculated accordingly.

3.2 Deep Belief Network (DBN)

DBN is constructed with a stack of Restricted Boltzmann Machines (RBM). RBM is based on the Markov Random Field (MRF) and has two units: binary stochastic hidden unit, and binary stochastic visible unit. It is not mandatory for the unit to be a Bernoulli random variable, and it can in fact have any distribution in the exponential family [14]. Besides, there are connections between hidden to visible and visible to hidden layers, but there is no connection between hidden-to-hidden or visible-to-visible units. The pictorial representation of RBM and DBN are shown in Figure 5.

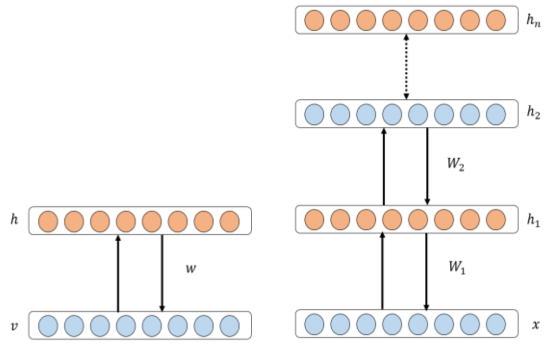

Figure 5. Block diagram for RBM (left) and DBN (right)

The symmetric weights on the connections and biases of the individual hidden and visible units have been calculated based on a probability distribution over the binary state vector of *v* for the visible units via an energy function. The RBM is an energy-based undirected generative model which uses a layer of hidden variables to model the distribution over the visible variable in the visible units [15]. In the undirected model of the interactions between the hidden and visible variables, both units are used to confirm that the contribution of the probability term to posterior over the hidden variables is approximately factorial, which greatly facilitates inference [16].

An energy-based model means that the likely distribution over the variables of interest is defined through an energy function. It can be composed from a set of observable variables $V = \{v_i\}$ and a set of hidden variables $H = \{h_i\}$ where i is the node in the visible layer and j is the node in the hidden layer. It is restricted in the sense that there are no visible-visible or hidden-hidden connections. The values correspond to "visible" units of the RBM because their states are observed; the feature detectors correspond to "hidden" units. A joint configuration, (v, h) of the visible and hidden units has an energy given by [14]:

$$E(v, h; \theta) = -\sum_i a_i v_i - \sum_j b_j h_j - \sum_i \sum_j v_i \; w_{i,j} \; h_j \tag{3}$$

where $\theta = (w, b, a)$, v_i and h_j are the binary states of visible unit i and hidden unit j, a_i, b_j are their biases and w_{ij} is the symmetric weight in between visible and hidden units. The network assigns a probability to every possible pair of a visible and a hidden vector via this energy function as

$$p(v, h) = \frac{1}{Z} e^{-E(v,h)} \tag{4}$$

where the "partition function" Z is given by summing over all possible pairs of visible and hidden vectors as follows:

$$Z = \sum_{v,h} e^{-E(v,h)}. \tag{5}$$

The probability which the network assigns to a visible vector, v, is generated through the summation over all possible hidden vectors as

$$p(v) = \frac{1}{Z} \sum_h e^{-E(v,h)}. \tag{6}$$

The probability the network assigns to a training image can be improved by adjusting the symmetric weights and biases to lower the energy of that image and to increase the energy of other images, especially those that have low energies, resulting in a huge contribution for the partitioning function. The derivative of the *log* probability of a training vector with respect to symmetric weight is remarkably simple, computed as

$$\frac{\partial logp(v)}{\partial w_{ij}} = \langle v_i h_j \rangle_{data} - \langle v_i h_j \rangle_{model} \tag{7}$$

where the angular brackets are used to represent the expectations under the distribution specified by the subscript that follows. It leads to a very simple learning rule for performing stochastic steepest ascent in the *log* probability on the training data

$$w_{ij} = \varepsilon \left(\langle v_i h_j \rangle_{data} - \langle v_i h_j \rangle_{model} \right) \tag{8}$$

where ε is a learning rate. Due to no direct connectivity between hidden units in an RBM, it is easy to get an unbiased sample of $\langle v_i h_j \rangle_{data}$. Given a randomly selected training image, v, the binary state h_j of each hidden unit j is set to 1 with the probability

$$p(h_j = 1|v) = \sigma(b_j + \sum_i v_i w_{ij}) \tag{9}$$

where $\sigma(x)$ is the logistic sigmoid function $1/(1 + e^{(-x)})$, $and\ v_i h_j$ is then an unbiased sample. As there are no direct connections between visible units in an RBM, it is also easy to get an unbiased sample of the state of a visible unit, given a hidden vector

$$p(v_i = 1|h) = \sigma(a_i + \sum_j h_j w_{ij}) . \tag{10}$$

It is much more difficult, however, to generate an unbiased sample of $\langle v_i h_j \rangle_{model}$. It can be done in the beginning at any random state of visible layer and by performing alternative Gibbs sampling for a very long period. Gibbs sampling consists of updating all the hidden units in parallel using Eq. (9) in one alternating iteration followed by updating all the visible units in parallel using Eq. (10).

A much faster learning procedure, however, has been proposed by Nair and Hinton [9]. This approach starts by setting the states of the visible units to a training vector. Then the binary states of the hidden units are all computed in parallel according to Eq. (9). Once binary states have been selected for the hidden units, a “reconstruction” is generated by setting each v_i to 1 with a probability given by Eq. (10). The change in a weight matrix can be written by

$$\Delta w_{ij} = \varepsilon \left(\langle v_i h_j \rangle_{data} - \langle v_i h_j \rangle_{recon} \right) , \tag{11}$$

a simplified version of the same learning rule that uses the states of individual units. The pairwise products approach, however, is used for the biases. The learning rule closely approximates the gradient of another objective function called the Constrictive Divergence (CD) [15] which differs from Kullback-Liebler divergences. It works well, however, to achieve better accuracy in many applications. CD is used to denote learning using *n* full steps of alternating Gibbs sampling.

The pre-training procedure with RBM is utilized to initialize the weight of the deep neural network, which is discriminatively fine-tuned by back-propagating error derivative. The sigmoid function is used as an activation function for this implementation. For the Deep Neural Networks (DNN) implementation, we have just used a traditional neural network with multiple hidden layers.

4. DATABASE AND EXPERIMENTAL RESULTS

4.1 Database

A database with 360 images was created from the set of 372 images mentioned in Section 2. The original data dimensions are 1300×1100 obtained from a NIF camera. Images were manually cropped to include the desired region to a 32×32 size. The images are single-channel gray-scale images. The dataset is split into two groups; one set is used for training of different deep-learning techniques including CNN, DBN and DNN. The training set contains 300 samples. The remaining set of 60 images are used for testing in this implementation. Some of the example images from the database are shown in Figure 6.

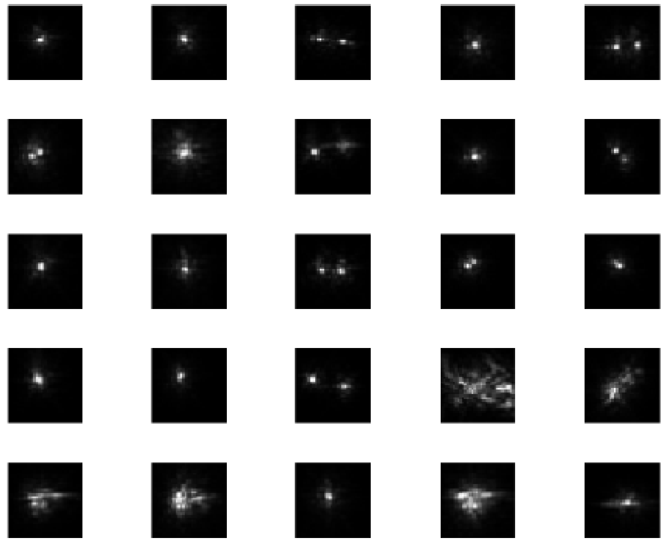

Figure 6. Example image from final dataset

4.2 Experimental results

In this work, we have classified two classes of composite optical beams using CNN, DBN, DNN and SVM [10]. We have used a simple architecture of CNN in this implementation. The network has six layers including input and output or classification layers, with two convolutional and sub-sampling (pooling) layers, and one fully connected layer. In the first experiment, we trained the network with 500 epochs, with batch size of 20, and learning rate of 1. The following figure shows the errors during training with respect to epoch for different methods. In the testing phase, we used the remaining 60 samples.

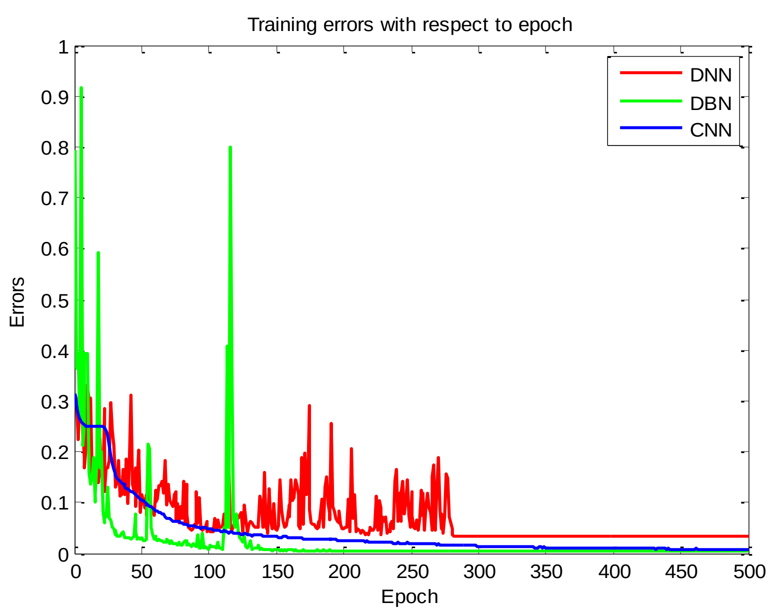

Figure 7. Errors during training with NN, DBN and CNN

To evaluate the performance of CNN, we trained and tested the system for 500 epochs. The blue line in Figure 7 shows the training errors with respect to the number of epoch for CNN. During the training, very smooth convergence behavior was observed in the case of CNN.   Figure 7 also shows the training errors with respect to the number of epochs for DBN in green. It can be clearly seen that after 200 epochs, error does not reduce much. The transfer learning approach is used for implementing DBN. For implementing DBN, we considered the structure of 1024->500->100->2, where 1024 is the number of input neurons, 500 and 100 are the number of hidden neurons, and 2 is the number of neurons in the outputs layer. The DBN is pre-trained with the unsuprevised feature-learning approach of RBM, which generates the initital weights, and the whole network is fine-tuned with a neural network with the backpropagation technique. The visualization of features learned during training using DBN is shown in Figure 8.

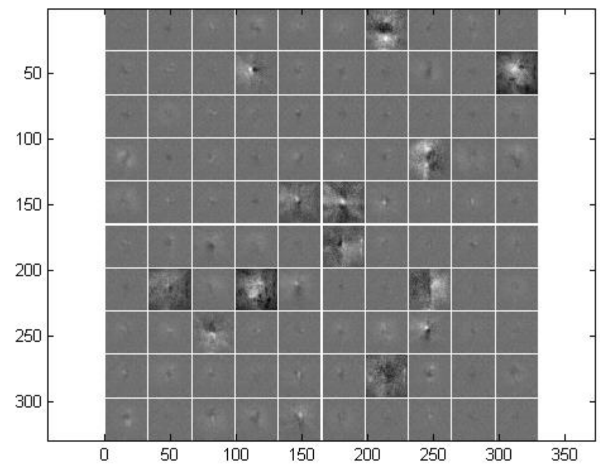

Figure 8. Visualization of features learned with DBN

Furthermore, we have implemented a DNN-based beam-classificaiton system. The DNN consists of architecture of 1024->512->100->2. where the DNN structure utilizes about 1024 input neurons, 512 and 100 neurons in the second and third hidden layers, and 2 neurons in the classification layer. The whole experiment is conducted for 500 epochs, with a batch size of 20 and a learning rate of 1. The red line in Figure 7 shows the training errors with respect to the epochs for the DNN technique. A very stable behavior is observed after around 275 epochs, which indicates that the eorror does not change after that particualr iteration. Moreover, SVM is implemented for beam classificiton for comparing against deep-learning techniques.

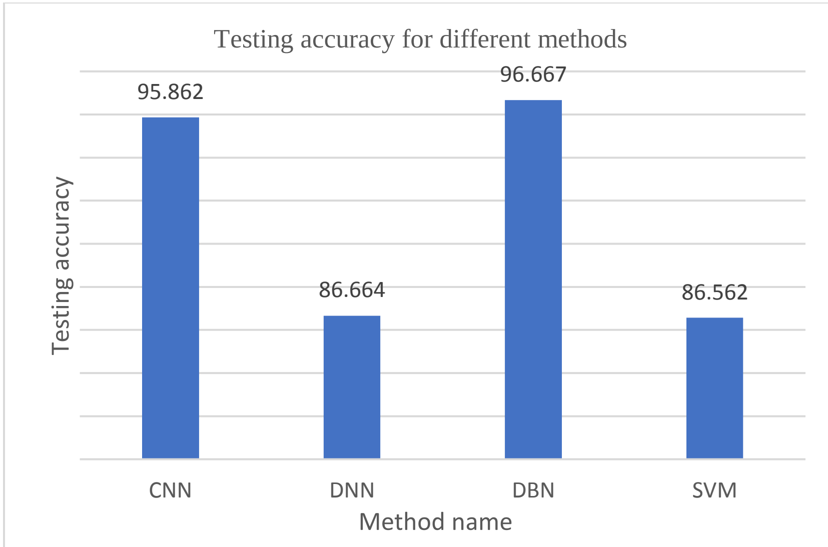

Figure 9. Testing accuracy for different methods

We have tested this method with 60 randomly selected testing samples. The bar graph in Figure 9 shows the average testing accuracy for times with CNN, DNN, DBN, and SVM. The experimental testing result shows about 95.86% testing accuracy for CNN. We have achieved about 86.66% classification accuracy for the DNN approach. The better accuracy of about 96.67%, however, is achieved using DBN which is pretrained with RBM and finetuned with NN. The SVM shows about 86.56% classification accuracy as testing accuracy for beam classification.

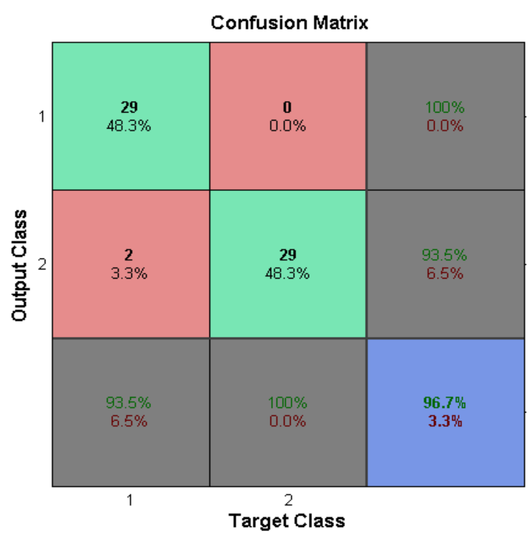

Figure 10. Confusion matrix for beam classification using DBN.

The confusion matrix for the highest classification accuracy in the testing phase using DBN is shown in Figure 10. From the figure, it can be clearly observed that out of 60 samples, 29 samples are classified as first and second class, respectively. Two samples, however, are misclassified as class two as shown in Figure 9. The overall testing accuracy shown in Figure 8 is 96.7%.

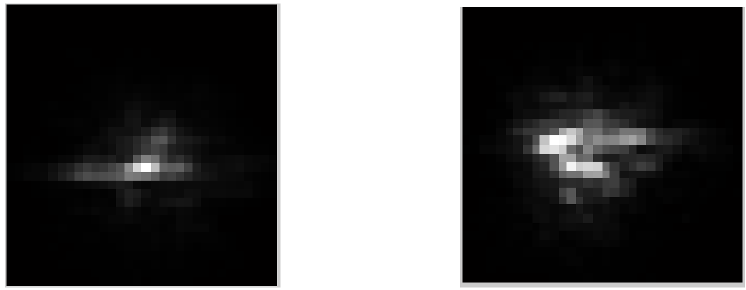

Figure 11. Misclassified images: actual class one, classified as class two

4.3 Introspection

Deep learning is a data-driven learning approach. Due to the small number of training and testing samples, the deep learning approach provided reasonable recognition accuracy. If the number of training samples is increased, however, the deep-learning-based approaches will provide even better accuracy compared to any traditional machine-learning approaches. Another comparison with feature-learning-based approaches is that the CNN has multiple layers of feature extraction and selection in multiple levels. The second feature extraction layer (convolution and subsampling) combines multiple features from the first layer and aggregates them into a more complex feature relationship layer. The final completely connected layers make class decisions by combining sets of second-layer features.

5. CONCLUSION

In this work, we have implemented different deep learning techniques for classification of composite optical laser beams. The experimental results show 95.86%, 86.66%, 96.67%, and 86.56% testing accuracy using CNN, DNN, DBN and SVM, respectively. The best classification accuracy is observed using Deep Belief Network (DBN) methods compared to other techniques. In the future, we would like to implement this solution with a transfer-learning approach [17]. In addition, we would like to implement this problem on a Neuromorphic system called IBM's TrueNorth system [18].

6. ACKNOWLEDGEMENT

The authors AASA and ZA will like to acknowledge the help of Judy Liebman, Lisa Belk and Sylwia Hamilton, for constructive feedback and improving the readability of this article significantly. This work performed under the auspices of the U.S. Department of Energy by Lawrence Livermore National Laboratory under Contract DE-AC52-07NA27344. This paper is released as LLNL-CONF-737645.

REFERENCES

[1] Mark Bowers, Jeff Wisoff, Mark Herrmann, Tom Anklam, Jay Dawson, Jean-Michel Di Nicola, Constantin Haefner, Mark Hermann, Doug Larson, Chris Marshall, Bruno Van Wonterghem and Paul Wegner, "Status of NIF laser and high-power laser research at LLNL," Proceedings Volume 10084, High Power Lasers for Fusion Research IV; 1008403 (2017)

[2] Mary L. Spaeth, Kenneth R. Manes, M. Bowers, P. Celliers, J.-M. Di Nicola, P. Di Nicola, S. Dixit, G. Erbert, J. Heebner, D. Kalantar, O. Landen, B. MacGowan, B. Van Wonterghem, P. Wegner, C. Widmayer & S. Yang, "National Ignition Facility Laser System Performance," Fusion Science and Technology Vol. 69, 366-394 (2016).

[3] C. Haefner, J. E. Heebner, J. Dawson, S. Fochs, M. Shverdin, J.K. Crane, K. V. Kanz, J. Halpin, H. Phan, R. Sigurdsson, W. Brewer, J. Britten, G. Brunton, B. Clark, M. J. Messerly, J. D. Nissen, B. Shaw, R. Hackel, M. Hermann, G. Tietbohl, C. W. Siders and C.P.J. Barty, "Performance Measurement of the Injection Laser System Configured for Picosecond Scale Advanced Radiographic Capability," The Sixth International Conference on Inertial Fusion Sciences and Applications, Journal of Physics: Conference Series 244, 032005 (2010).

[4] J. R. Rygg, O. S. Jones, J. E. Field, M. A. Barrios, L. R. Benedetti, G. W. Collins, D. C. Eder, M. J. Edwards, J. L. Kline, J. J. Kroll, O. L. Landen, T. Ma, A. Pak, J. L. Peterson, K. Raman, R. P. Town, D. K. Bradley, “2D X-ray radiography of imploding capsules at the national ignition facility,” Phys Rev Lett., 112, p. 195001 (2014).
[5] Richard Leach, Abdul A. Awwal, Roger Lowe-Webb, Victoria Miller-Kamm, Charles Orth, Randy Roberts, Karl Wilhelmsen, “Image processing for the Advanced Radiographic Capability (ARC) at the National Ignition Facility,” Proc. SPIE. 9970, Optics and Photonics for Information Processing X, p 99700M (2016).
[6] A. A. S. Awwal, K. Wilhelmsen, R. R. Leach, V. Miller-Kamm, S. Burkhart, R. Lowe-Webb, and S. Cohen, “Autonomous monitoring of control hardware to predict off-normal conditions using NIF automatic alignment systems,” Fusion Engineering and Design, Volume 87, 2140–2144 (2012).
[7] Y. LeCun, L. Bottou, Y. Bengio, and P. Haffner, “Gradient-based learning applied to document recognition,” Proceedings of the IEEE, vol. 86, no. 11, pp. 2278–2324 (1998).
[8] Alex Krizhevsky, Ilya Sutskever, and Geoffrey E. Hinton. "Imagenet classification with deep convolutional neural networks." *Advances in neural information processing systems*, Vol. 25, pp. 1097-1105 (2012).
[9] V. Nair and G. Hinton, “Rectified linear units improve restricted boltzmann machines,” Proceedings of the 27th International Conference on Machine Learning (ICML-10), 807-814 (2010).
[10] Yichuan Tang “Deep Learning using Linear Support Vector Machines” proceedings of International Conference on Machine Learning in 2013.
[11] Kunihiko Fukushima and Sei Miyake. "Neocognitron: A self-organizing neural network model for a mechanism of visual pattern recognition." *Competition and cooperation in neural nets*. Springer, Berlin, Heidelberg, 267-285 (1982)
[12] Kaiming He, et al. "Delving deep into rectifiers: Surpassing human-level performance on imagenet classification." *Proceedings of the IEEE international conference on computer vision*, pp. 1026-1034 (2015).
[13] Abdel-rahman Mohamed, George E. Dahl, and Geoffrey Hinton, “Acoustic modeling using deep belief networks,” Audio, Speech, and Language Processing, IEEE Transactions on 20, 14-22 (2012)
[14] M. Welling, M. Rosen-Zvi, and G. E. Hinton, “Exponential family harmoniums with an application to information retrieval,” in *Proc. NIPS* 17 (2004).
[15] A. K. Noulas and B.J.A. Kröse, “Deep Belief Networks for Dimensionality Reduction,” Belgian-Netherlands Conference on Artificial Intelligence, pp. 185-191 (2008).
[16] L. McAfee, “Document Classification using Deep Belief Nets,” CS224n, Sprint 2008.
[17] G. Mesnil, Y. Dauphin, et al. "Unsupervised and transfer learning challenge: a deep learning approach." *Proceedings of ICML Workshop on Unsupervised and Transfer Learning*, Vol. 27, pp. 97-111 (2012).
[18] Filipp Akopyan, et al. "Truenorth: Design and tool flow of a 65 mw 1 million neuron programmable neurosynaptic chip." *IEEE Transactions on Computer-Aided Design of Integrated Circuits and Systems* 34 1537-1557 (2015)